American Journal of Pathology, Vol. 164, No. 5, May 2004

Activation of the *GLI* Oncogene through Fusion with the β-Actin Gene (*ACTB*) in a Group of Distinctive Pericytic Neoplasms

Pericytoma with t(7;12)

Anna Dahlén,* Christopher D. M. Fletcher,† Fredrik Mertens,* Jonathan A. Fletcher,† Antonio R. Perez-Atayde,‡ M. John Hicks,§ Maria Debiec-Rychter,¶ Raf Sciot,‖ Johan Wejde,** Rikard Wedin,†† Nils Mandahl,* and Ioannis Panagopoulos*

From the Department of Clinical Genetics, University Hospital, Lund, Sweden; the Departments of Pathology** and Orthopedics,†† Karolinska Hospital, Stockholm, Sweden; the Center of Human Genetics¶ and the Department of Pathology,‖ University of Leuven, Leuwen, Belgium; the Department of Pathology,† Brigham and Women's Hospital, Boston, Massachusetts; the Department of Pathology,‡ Children's Hospital, Boston, Massachusetts; and the Department of Pathology,§ Texas Children's Hospital, Houston, Texas*

Activation of the *GLI* oncogene is an important step in the sonic hedgehog signaling pathway, and leads to, eg, tissue-specific cell proliferation during embryogenesis. *GLI* activity in adult tissues is restricted, but has been identified in various neoplasms, as a result of mutations in the *PTCH* (patched) or *SMOH* (smoothened) genes, encoding components of the sonic hedgehog pathway, or by amplification of *GLI*. Herein, we present a new mechanism of *GLI* activation through fusion with the β-actin gene (*ACTB*) in five histologically distinctive soft tissue tumors showing a t(7;12)(p21-22;q13-15) and a pericytic phenotype. Each was composed of a perivascular proliferation of monomorphic short spindle cells that stained positively for smooth muscle actin and laminin and that showed pericytic features by electron microscopy. To date, with a median follow-up of 24 months, none has behaved in an aggressive manner. Molecular genetic analysis showed that the translocation in all cases resulted in a fusion transcript including the 5′-part of *ACTB* and the 3′-part of *GLI*. The DNA-binding zinc finger domains of *GLI* were retained in the fusion transcripts and it is likely that the replacement of the promoter region of *GLI* with that of the ubiquitously expressed *ACTB* gene leads to deregulation of *GLI* expression and its downstream target genes. ***(Am J Pathol 2004, 164:1645–1653)***

Soft tissue sarcomas constitute a clinically and histologically heterogeneous group of malignant neoplasms, which sometimes are difficult to distinguish from each other or from their benign counterparts.[1] The cytogenetic picture is equally variable, but the identification of recurrent tumor-specific translocations and the gene rearrangements resulting from these translocations has added significantly to diagnostic precision. Comparable reciprocal translocations, albeit apparently often less specific, have also been identified in some benign mesenchymal neoplasms, such as lipomas and leiomyomas.[2,3] Furthermore, the molecular genetic characterization of these recurrent cytogenetic rearrangements has also enabled a better understanding of the genetic mechanisms underlying the development of sarcomas.[2,3]

A characteristic feature of sarcoma-associated translocations is that they result in fusion genes by the joining together of the 5′-part of one gene with the 3′-part of another gene. Typically, at least one of the two genes involved encodes a transcription factor, but also translocations leading to constitutive activation of growth factors or growth factor receptors have been identified.[2]

In the present study, we report the finding of a novel fusion gene in five spindle cell tumors with distinctive pericytic features. Lesions of this type seem previously to be unrecognized as a discrete entity. In all of them, cytogenetic analysis revealed a t(7;12)(p21-22;q13-15), that at molecular genetic investigation was found to result in fusion of the *ACTB* (β-actin) and *GLI* (glioma-associated oncogene homologue 1) genes, neither of which has previously been implicated in fusion genes in sarcomas or other neoplasms.

Supported by the Swedish Children's Cancer Foundation, the Swedish Cancer Society, and the Gunnar Nilsson Cancer Fund.

Accepted for publication January 21, 2004.

Address reprint requests to Anna Dahlén, Department of Clinical Genetics, University Hospital, SE-221 85 Lund, Sweden. E-mail: anna.dahlen@klingen.lu.se.

Table 1. Panel of Antibodies for Immunohistochemical Analysis

Antigen	Clone	Dilution	Antigen retrieval	Source
SMA	1A4	1:20000	None	Sigma, St. Louis, MO
Muscle actin	HHF35	1:500	None	DAKO, Carpinteria, CA
CK (AE1/AE3)	AE1/AE3	1:200	10 minute protease	DAKO
CK 8/18	CAM 5.2	1:100	10 minute protease	Becton Dickinson, San Jose, CA
Desmin	D33	1:500	None	DAKO
CD10	56C6	1:10	30 minute microwave	Novocastra, Newcastle, UK
Laminin	Polyclonal	1:1500	30 minute protease	DAKO
COLL IV	CIV 22	1:200	20 minute protease	DAKO
S-100	Polyclonal	1:3000	None	DAKO
CALDES	h-CD	1:300	30 minute microwave	DAKO
Melanoma (HMB45)	HMB45	1:400	None	DAKO
EMA	E29	1:200	None	DAKO
CD34	Qbend 10	1:400	None	DAKO
CD31	JC/70A	1:40	20 minute protease	DAKO
D6	D2-40	1:100	None	Signet Lab, Dedham, MA
KIT	Polyclonal (A4502)	1:250	None	DAKO
PR	PgR 636	1:200	30 minute microwave	DAKO

Abbreviations: SMA, smooth muscle actin; CK, cytokeratin; COLL IV, collagen type IV; CALDES, caldesmon; EMA, epithelial membrane antigen; PR, progesterone receptor.

Materials and Methods

Pathological Analysis

The five tumors included in this study were all selected initially for further molecular genetic and histopathological analyses on the basis of their cytogenetic features, ie, the presence of a translocation t(7;12)(p21-22;q13-15). One case was the subject of a previous case report.[4] Four μm hematoxylin and eosin-stained sections of all cases were examined and immunohistochemical studies were performed in all cases, using the Envision Plus detection system (DAKO, Carpinteria, CA). The antibodies, clones, dilutions, pretreatment conditions, and sources are listed in Table 1. Appropriate positive and negative controls were used throughout. Electron microscopy was performed on three tumors (cases 2, 3, and 5) in which fresh material had been suitably fixed in glutaraldehyde.

Cytogenetic and Fluorescence in Situ *Hybridization (FISH) Analyses*

Cell culturing, harvesting, and G-banding were performed as described,[4,5] and the karyotypes were written according to the recommendations of the International System for Human Cytogenetic Nomenclature (ISCN).[6] The cytogenetic features of case 5 have been reported previously.[4]

Material for metaphase and interphase FISH analysis was available for cases 1 and 5, respectively. To identify the chromosomal breakpoints in case 1, 20 bacterial artificial chromosome (BAC) probes spanning 7p21-22 or 12q13 were selected from the NCBI Map Viewer (http://www.ncbi.nlm.nih.gov/mapview), the Ensembl Genome Browser (http://www.ensembl.org) and the UCSC Human Genome Browser (http://www.genome.ucsc.edu). It should be noted that based on our FISH findings and polymerase chain reaction (PCR) results showing that it contains the *ACTB* locus, BAC RP11-1275H24 was substantially larger than the ~85 kb reported at the NCBI Nucleotide Browser. Whole chromosome painting probes (Vysis, Downers Grove, IL) were also used to identify material from chromosomes 7 and 12. The BAC probes were labeled with Cy3-dCTP (Amersham, Buckinghamshire, UK), FluorX-dCTP (Amersham) or biotin-16-dUTP (Roche, Mannheim, Germany), using the Megaprime DNA labeling system (Amersham). The FISH treatments and analyses were performed as described.[7]

Molecular Genetic Analyses

Total RNA was extracted from frozen tissue (cases 1 to 4) or cell cultures (case 5), using the Trizol-reagent according to the manufacturer's recommendations (Gibco BRL, Täby, Sweden). For the cDNA synthesis, 5 μg of total RNA were reverse-transcribed in a 20-μl reaction, containing 50 mmol/L Tris-HCl, pH 8.3 (at 25°C), 75 mmol/L KCl, 3 mmol/L $MgCl_2$, 10 mmol/L dithiothreitol, 1 mmol/L of each dNTP, 0.5 pmol/L random hexamers, 28 U RNase inhibitor (RNA guard, Amersham), and 400 U M-MLV reverse transcriptase (Invitrogen, Stockholm, Sweden). The reaction was incubated for 1 hour at 37°C, followed by 5 minutes at 65°C. As an internal quality control, 1 μl of cDNA was amplified by PCR using *ABL1*-specific primers.

PCR and Sequence Analyses

Reverse transcriptase (RT) PCR was used for the detection of the *ACTB-GLI* and the reciprocal *GLI-ACTB* fusion transcripts. The nucleotide sequences for all primers used for PCR amplification and sequence analyses are presented in Table 2. One μl of cDNA was used as template for PCR, and all PCRs described below were performed under the same conditions, ie, the 50-μl reaction contained 20 mmol/L Tris-HCl, 50 mmol/L KCl, 1.25 mmol/L $MgCl_2$, 0.8 mmol/L dNTPs, 0.5 μmol/L of each primer, and 1 U Platinum *Taq*DNA Polymerase (Invitrogen). After an initial denaturation for 5 minutes at 95°C, 30 cycles of 1 minute at 94°C, 1 minute at 60°C, and 1

Table 2. Primers for RT-PCR and Direct Sequencing

Primer*	Sequence	Position	Accession no.
GLI336F	5′-ACCTCTGTCGGATGCCAGCCTGG	336–358	NM_005269
GLI412F	5′-TCGCGATGCACATCTCCAGGAGG	412–434	NM_005269
GLI520F	5′-TCCTTTGGGGTCCAGCCTTGTGG	520–542	NM_005269
GLI577R	5′-AAGGGTCCCCGGGACTGAGGATG	599–577	NM_005269
GLI628R	5′-CGGCACTTGCCAACCAGCATGTC	650–628	NM_005269
GLI720R	5′-AGGTCCTCCCGCCCATCCAGC	740–720	NM_005269
GLI868R	5′-GTGGCACACGAACTCCTTCCGCTC	891–868	NM_005269
GLI938R	5′-TCTGCGCATGTGAACCACCAGCA	960–938	NM_005269
GLI1246R	5′-GCCGTTTGGTCACATGGGCGTC	1267–1246	NM_005269
GLI1389R	5′-CCCCAGGGCTTGGCTGTGGC	1408–1389	NM_005269
GLI1477R	5′-TGCCCCCTGCATTGCCAGTCAT	1498–1477	NM_005269
ACT18F	5′-CACAGAGCCTCGCCTTTGCCGA	18–39	NM_001101
ACT61F	5′-CCGCCAGCTCACCATGGATGATG	61–83	NM_001101
ACT80F	5′-GATGATATCGCCGCGCTCGTCG	80–101	NM_001101
ACT106F	5′-CAACGGCTCCGGCATGTGCAA	106–126	NM_001101
ACT288F	5′-AGCACGGCATCGTCACCAACTGG	288–310	NM_001101
ACT351F	5′-AGCTGCGTGTGGCTCCCGAGG	351–371	NM_001101
ACT520R	5′-CACCGGAGTCCATCACGATGCCA	542–520	NM_001101
ACT594R	5′-AGCCAGGTCCAGACGCAGGATGG	616–594	NM_001101

*F, forward primer; R, reverse primer.

minute at 72°C were run using a PCT-200 DNA Engine (MJ Research, Waltham, MA), followed by a final extension for 10 minutes at 74°C. For the nested RT-PCR, 1 μl of the first PCR products was used as template.

A total of 8 *ACTB*-specific, and 11 *GLI*-specific primers were selected, to allow a precise mapping of the fusion transcripts (Figure 1a and Table 2). In cases 1 to 4, the *ACTB-GLI* fusion transcripts were amplified with primer pairs ACT61F-GLI868R, ACT18F-GLI1246R, ACT61F-GLI1477R, and ACT61F-GLI938R, respectively. A reciprocal *GLI-ACTB* fusion was detected by nested PCR in case 1, using the primer pair GLI412F-ACT594R, in the first round of PCR, and GLI520F-ACT520R for the second. In case 5, nested PCR was required for the detection of all fusion sequences. The *ACTB-GLI* and *GLI-ACTB* fusion transcripts were amplified in a first round of RT-PCR with primer pairs ACT80F-GLI1246 and GLI336-ACT594R, respectively. For nested PCR, the corresponding primer pairs ACT106F-GLI868R and GLI412F-ACT520R were used.

All PCR products (15 μl) were analyzed on 1.5% agarose gels stained with ethidium bromide. For sequence analysis, the band corresponding to the expected PCR product was excised, purified using the QIAquick gel extraction kit (Qiagen, Hilden, Germany), and sequenced in a 20-μl reaction with various primers (Table 2), using the dideoxy procedure with an ABI Prism BigDye terminator cycle sequencing ready reaction kit on the Applied Biosystems (Foster City, CA) model 310 DNA sequencing system. The BLAST software (http://www.ncbi.nlm.nih.gov/blast) was used for the analysis of *ACTB* [accession numbers: NM_001101 (mRNA), M10277 (complete cds)], and *GLI* [accession number: NM_005269 (mRNA)] sequence data.

Results

Clinicopathological Features

Clinical data are summarized in Table 3. All tumors were primary lesions, three being located in the tongue and one each in the stomach and calf. Three patients were female and two were male, ranging in age at presentation from 11 to 65 years (median, 27 years). Tumor size ranged from 0.8 to 5.5 cm (median, 2.4 cm). Two of the tongue lesions (cases 2 and 3) were treated with preoperative chemotherapy with no clear evidence of response. All were locally resected, with tumor-positive resection margins in cases 3 and 5. Follow-up so far, ranging from 22 to 120 months (median, 24 months), has revealed no evidence of recurrence or metastasis.

Histologically each tumor showed remarkably similar morphology, seemingly somewhat distinct from any currently well-defined entity. The tumors had a multilobulated, infiltrative growth pattern and were each composed of uniform spindle-shaped cells with small amounts of pale eosinophilic cytoplasm and ovoid-to-tapered nuclei with vesicular chromatin and often a single small nucleolus (Figure 2, A and B). These spindle cells were consistently arranged around numerous small, thin-walled arborizing vessels, which were readily highlighted by immunopositivity for CD34 (Figure 2C). There was no significant cytological atypia or pleomorphism. Mitoses in all cases numbered less than 1 per 10 high-power fields. Three of the cases showed a focally myxoid stroma. In two cases there was prominent and multifocal subendothelial protrusion of tumor cells into vascular lumina (Figure 2D), in a manner reminiscent of myopericytic neoplasms. Two of the tongue lesions showed focal surface ulceration and the gastric lesion showed areas of stromal hemorrhage and hyalinization but no true tumor necrosis was seen in any case.

Immunohistochemical analysis (Table 4) revealed that tumor cells in all cases showed focal to extensive positivity for smooth muscle actin (Figure 2E), as well as multifocal pericellular positivity for laminin (Figure 2F), consistent with the presence of an external lamina. Three cases each also showed positivity for collagen type IV and for CD10. Staining for keratins, desmin, S-100 protein, and CD34 was consistently negative. One tumor

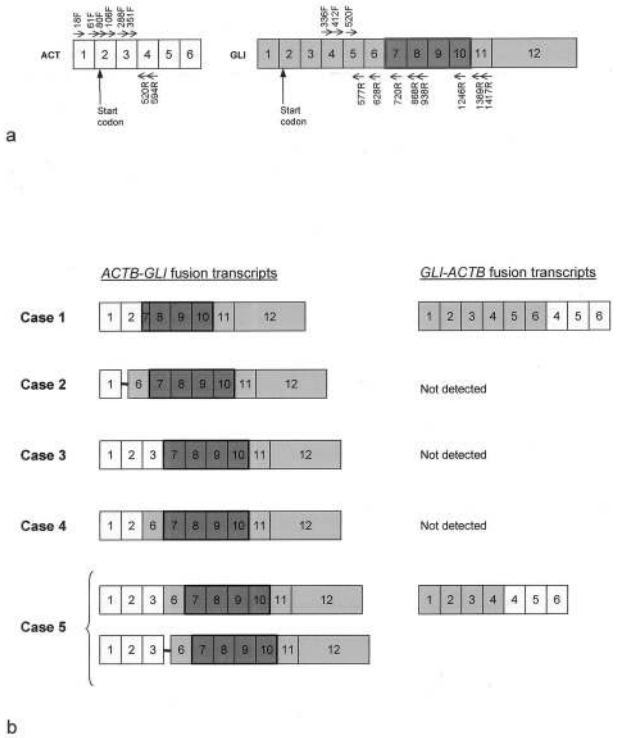

Figure 1. a: Position of the selected primers in relation to the *ACTB* and *GLI* cDNA sequences (see text and Table 1 for details). The exons as well as primer suffix and orientation (F, forward; R, reverse) are indicated. **b:** Schematic representation of the *ACTB-GLI* and *GLI-ACTB* fusion transcripts, detected by RT-PCR in five cases with a t(7;12)(p21-22;q13-15). Exons are illustrated as **boxes**, intronic material as **thick horizontal lines**. Exons 7 to 10 of *GLI*, encoding DNA-binding zink finger domains, are highlighted.

each showed cytoplasmic positivity for D2-40 (case 4) and focal epithelial membrane antigen positivity (case 1) of uncertain significance.

Three tumors examined ultrastructurally (cases 2, 3, and 5) each showed similar features (Figure 3). The tumor cells were closely arranged around capillary size vessels and exhibited short segments of external lamina, occasional intermediate-type junctions, cytoplasmic pools of free glycogen, subplasmalemmal thickenings, and bundles of thin filaments with focal densities at the cytoplasmic periphery. These findings indicate partial smooth muscle differentiation, as seen in modified smooth muscle cells including pericytes.

G-Band and FISH Analyses

All cases were cytogenetically analyzed after short-term culturing, and a t(7;12)(p21-22;q13-q15) was found in all cases, being the sole abnormality in two of them (Table 3). In case 1, metaphase FISH analysis with the 7p-specific probes RP11-1275H24 and RP11-93G19, and the 12q-specific probes RP11-181L23 and RP11-772E1 resulted in split signals in the t(7;12)-carrying cells (Figure 4a). On the corresponding normal homologues, intact signals were seen. In case 5, only interphase nuclei from cell cultures in passage 6 were available for FISH analysis. Hybridization with probes RP11-1275H24 and RP11-772E1 revealed split signals in ~1% (8 and 11 nuclei, respectively) of the nuclei (Figure 4a). Based on these FISH results, *ACTB* and *GLI* were considered potential target genes in 7p22 and 12q13, respectively (Figure 4, b and c).

Molecular Genetic Findings

RT-PCR with different combinations of *ACTB* forward and *GLI* reverse primers amplified cDNA fragments, strongly suggesting the presence of an *ACTB-GLI* fusion gene (Figure 5). Amplified products were analyzed by direct sequencing for an exact characterization of the corresponding fusion points. The molecular genetic findings are summarized in Figure 1b. Analyses regarding expression of the *FLJ11467* gene or a potential *FLJ11467-GLI* fusion gene were consistently negative (data not shown).

In case 1, the primer pair ACT61F-GLI868R amplified a 270-bp product in which *ACTB* exon 2 (nucleotide 196, NM_001101) was fused to nucleotide 758 within exon 7 of *GLI* (NM_005269). Insertion of a guanine at the breakpoint retained the open reading frame (Figure 6). In case 2, the primer pair ACT18F-GLI1246R amplified a 754-bp product corresponding to an *ACTB-GLI* fusion transcript containing *ACTB* intron 1 sequences. In this transcript, *ACTB* exon 1 and nucleotides 313 to 319 of *ACTB* intron 1 (M10277) were joined to nucleotides 1017 to 1043 of *ACTB* intron 1 (M10277), which in turn was fused to *GLI* exon 6 (nucleotide 613, NM_005269) (Figure 6). In case 3, the ACT61F-GLI1477 primer combination amplified an 1172-bp product corresponding to a fusion of *ACTB* exon 3 (nucleotide 436, NM_001101) to *GLI* exon 7 (nucleotide

Table 3. Clinical Data and Cytogenetic Findings

Case	Sex/age	Localization	Size*	Follow-up†	Karyotype
1	M /61	Calf	2	NED 24	45,XY,t(7;12)(p22;q13),inv(10)(p11q21)c,der(15;16)(q10;p10)[25]
2	F /27	Tongue	0.8	NED 60	46,XX,t(7;12)(p22;q13)[20]
3	M /11	Tongue	5	NED 22	45,XY,der(1)t(1;?7)(p36;p?22),add(2)(p25),add(5)(p15),add(6)(p?21.3),der(7)t(7;12)(p11.2;p11.2),der(7)t(7;12)(p21;q?15),−12[19]
4	F /65	Stomach	5.5	NED 24	46,XX,t(7;12)(?p22;?q15)[17]
5	F /12	Tongue	2.4	NED 120	46,XX,t(1;13)(p22;q21),t(7;12)(p22;q13)[20]

*Diameter in cm.
†Follow-up in months; NED, no evidence of disease.

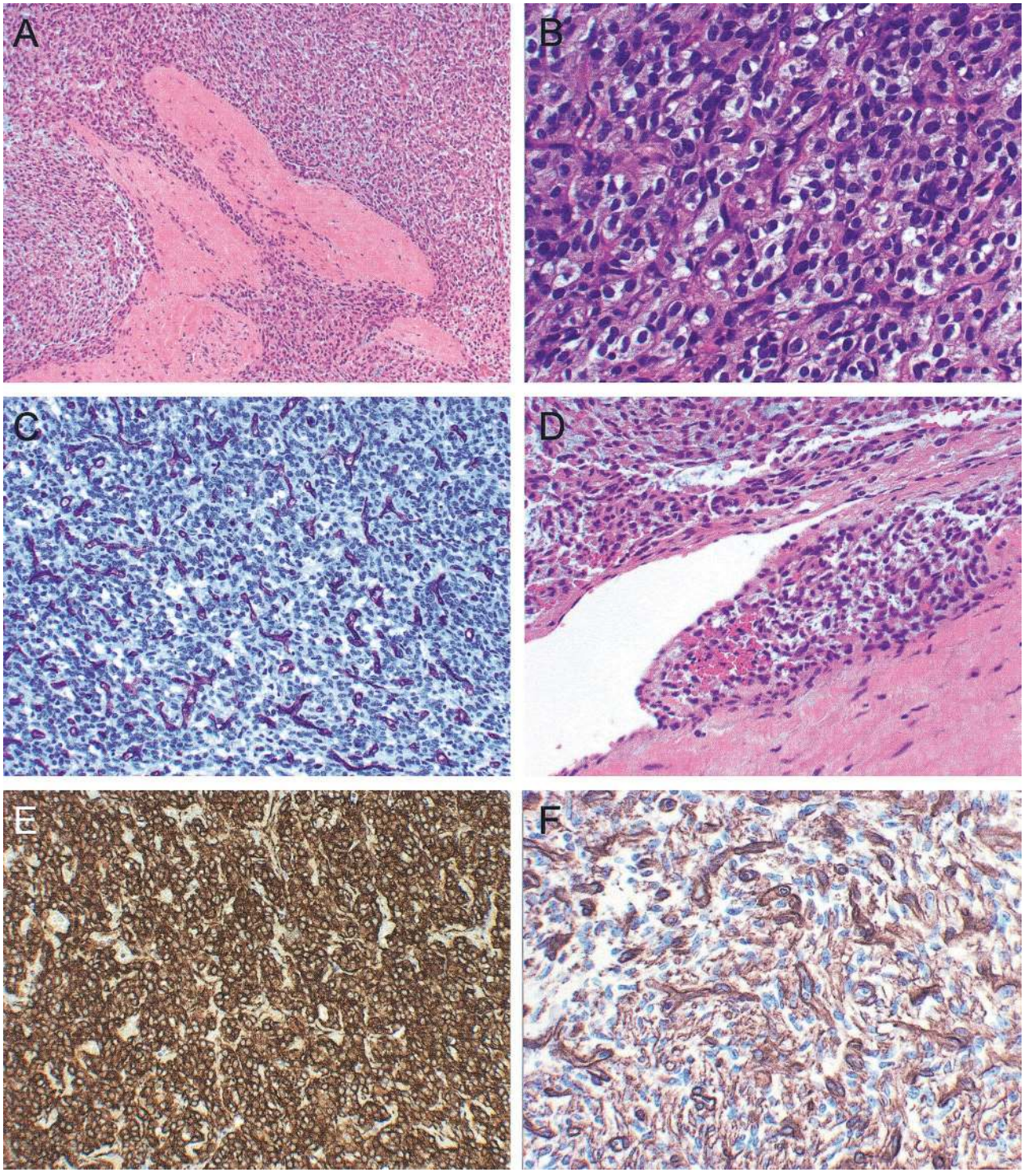

Figure 2. Tumors were composed of palely eosinophilic spindle-to-ovoid cells with a lobular/infiltrative margin (**A**). Tumor cells in each case were monomorphic and arranged around numerous thin-walled capillary vessels (**B**), which were better highlighted by immunostaining for CD34 (**C**). Subendothelial proliferation of tumor cells, as often seen in myopericytic tumors and mimicking vascular invasion, was seen in two cases (**D**). Tumor cells showed consistent, albeit variably prominent immunopositivity for smooth muscle actin (**E**) and there was pericellular positivity for laminin (**F**). Capillary vessel walls are also highlighted by laminin staining.

703, NM_005269) (Figure 6). In case 4, a 484-bp product was amplified with primer pair ACT61F-GLI938R, corresponding to a fusion of *ACTB* exon 2 (nucleotide 196, NM_001101) to *GLI* exon 6 (nucleotide 613, NM_005269) (Figure 6). Nested PCR was required for the amplification of *ACTB-GLI* fusion transcripts in case 5. Amplification with primer pair ACT80F-GLI1246R yielded no visible band at gel electrophoresis. Nested PCR with primer pair ACT106F-GLI868R resulted in the amplification of several bands (Figure 5), two of which were analyzed by direct

Table 4. Immunohistochemical Findings*

Case	SMA	HHF-35	CK	Desmin	CD10	Laminin	COLL IV	S100	CALDES	HMB45	EMA	CD34	D2-40
1	+	NP	−	−	NP	+ (focal)	NP	NP	−	NP	+ (focal)	NP	NP
2	+	NP	−	−	NP	+ (focal)	+ (focal)	−	NP	−	−	−	−
3	+ (focal)	NP	−	−	+	+ (focal)	+ (focal)	−	NP	−	−	−	−
4	+ (focal)	−	−	−	+	+	+	−	−	−	−	−	+
5	+ (focal)	−	−	−	+	+ (focal)	−	−	NP	−	NP	−	−

Abbreviations: NP, not performed; SMA, smooth muscle actin; CK, keratin; COLL IV, collagen type IV; CALDES, caldesmon; EMA, epithelial membrane antigen.

*Additional results not listed in the table above include negativity for progesterone receptor (cases 3 to 5), for CD31 (cases 1, 4), and for KIT (cases 4, 5).

sequencing. The first band (610 bp) corresponded to an in-frame fusion of *ACTB* exon 3 (nucleotide 436, NM_001101) to *GLI* exon 6 (nucleotide 613, NM_005216). Sequencing of the second band (712 bp) revealed an alternative transcript containing ACTB intron 3 sequences. Thus, in this transcript, *ACTB* exon 3 (nucleotide 1587, M10277), and nucleotides 1588 to 1592 of *ACTB* intron 3, were fused to nucleotides 1706 to 1604 of *ACTB* intron 3 (M10277), and joined to *GLI* exon 6 (nucleotide 613, NM_005269) (Figure 6). Results from genomic PCR were in good agreement with the RT-PCR findings in all five cases (data not shown).

Reciprocal transcripts were detected by nested PCR in cases 1 and 5. Amplification with primer pairs GLI412F-ACT594R and GLI336F-ACT594R, in cases 1 and 5, respectively, did not yield any visible product at gel electrophoresis, but nested PCR with the corresponding primer pairs GLI520F-ACT520R (case 1) and GLI412F-ACT520R (case 5), amplified fragments that were analyzed by direct sequencing. In case 1, the amplified 289-bp fragment corresponded to a fusion of *GLI* exon 6 (nucleotide 702, NM_00592) to *ACTB* exon 4 (nucleotide 434, NM_001101) (Figure 6). In case 5, the amplified 162-bp fragment corresponded to a fusion of *GLI* exon 4 (nucleotide 467, NM_005269) with *ACTB* exon 4 (nucleotide 437, NM_001101) (Figure 6).

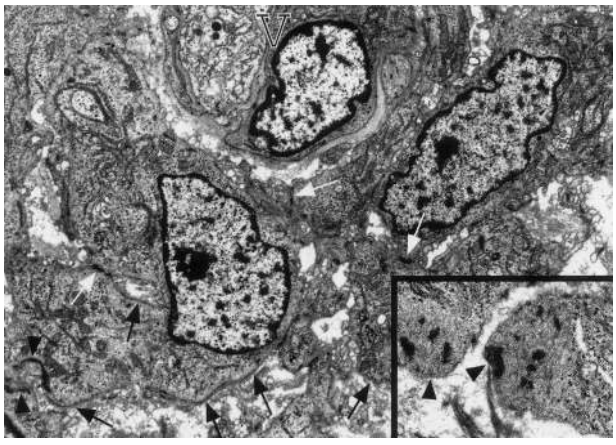

Figure 3. Electron microscopic examination closely apposed lesional cells arranged around small vessels (V). Tumor cells had prominent external lamina and subplasmalemmal densities (**black arrows**). Also noted were bundles of cytoplasmic myofilaments (**black arrowheads**) with focal densities, as well as intermediate-type intercellular junctions (**white arrowheads**). These appearances, in context, favor pericytic differentiation.

Discussion

We have identified a discrete group of previously uncharacterized neoplasms that are remarkably homogeneous at the morphological, cytogenetic, and molecular genetic levels. These lesions that, to date, seem benign (albeit with quite limited follow-up) have cytoarchitectural, immunohistochemical, and ultrastructural features highly suggestive of pericytic differentiation and it seems most likely that these lesions fall within the recently recognized spectrum of myopericytic neoplasms.[8] Arguably they could be regarded as the true hemangiopericytomas, but, given the loosely used manner in which the latter term has been used in the past 30 years and in view of the resulting confusion, then this terminology seems undesirable at least in the short term. In fact, in the new World Health Organization classification of soft tissue tumors, hemangiopericytoma has been discarded as a discrete entity and is regarded as synonymous with cellular examples of solitary fibrous tumor.[9] In these circumstances (and in line with the established trend in hematolymphoid neoplasia), we suggest the term "pericytoma with t(7;12)" for these lesions, thereby reflecting both their morphological and cytogenetic characteristics. Notably, this group of lesions, which was first identified through their shared karyotypic features, harbors not only a novel, seemingly tumor-specific chromosomal translocation but also a previously unrecognized mechanism of *GLI* activation.

Tumors that might enter the morphological differential diagnosis include cellular examples of solitary fibrous tumor (often termed "hemangiopericytoma" in the past), which have more patternless architecture, more prominent stromal collagen, larger branching vessels, and show consistent CD34 positivity; myofibroma(tosis), which generally has a biphasic appearance with fascicular myoid areas and is most frequent in young children; monophasic synovial sarcoma, which is more fascicular and shows immunopositivity for epithelial membrane antigen and/or keratin; and mesenchymal chondrosarcoma that shows more round cell morphology, greater nuclear atypia, and has foci of cartilaginous differentiation. An additional consideration could be metastatic endometrial stromal sarcoma, in which the vessels are more rounded (spiral arteriole-like) and which often shows focal keratin and desmin immunopositivity as well as consistent positivity for progesterone receptor.

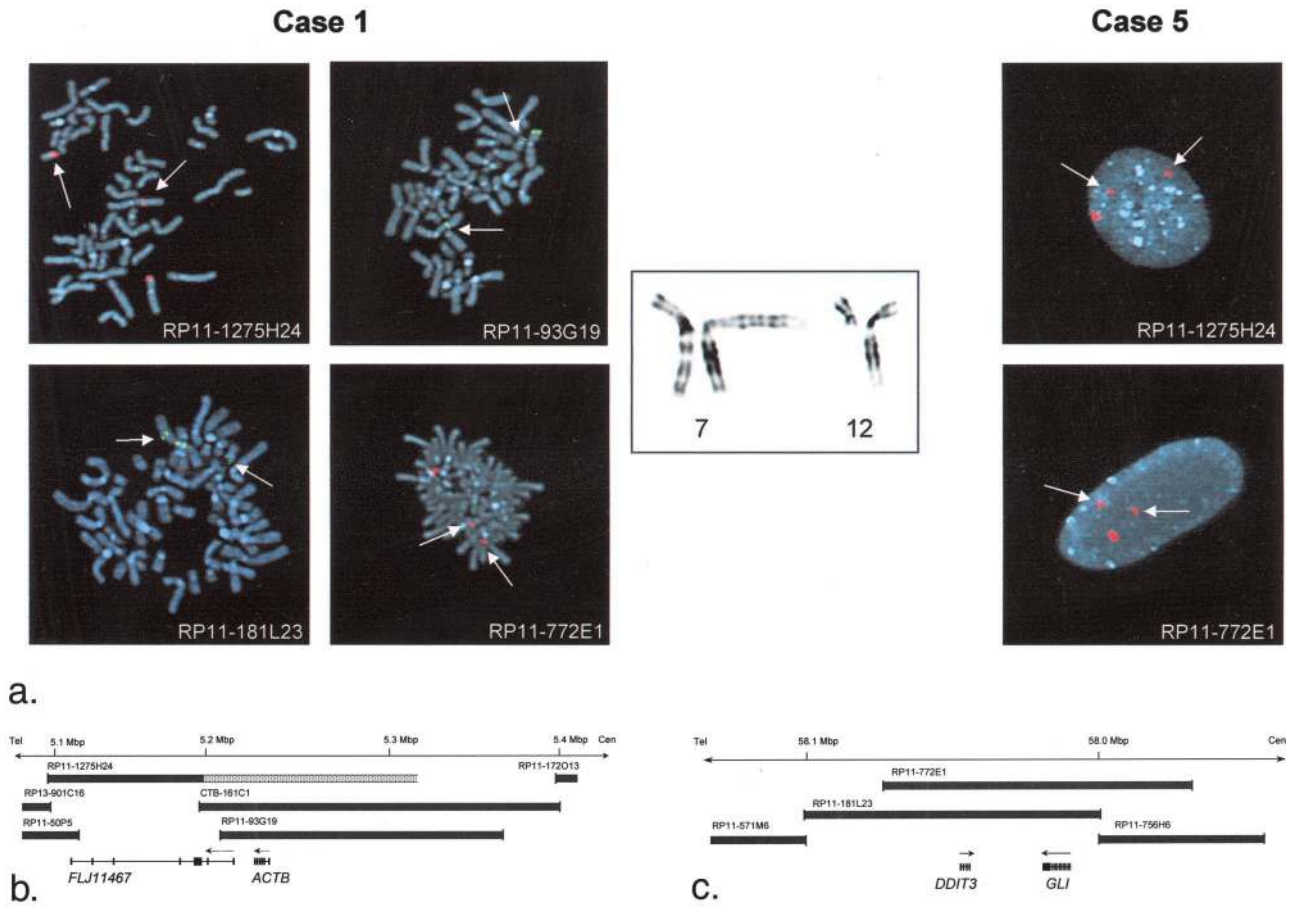

Figure 4. a: FISH images of cases 1 and 5, showing split signals (**arrows**) with the 7p22 (RP11-1275H24 and RP11-93G19)- and 12q13 (RP11-772E1 and RP11-181L23)-specific probes in cells with the t(7;12)(p22;q13), strongly suggesting that the translocation breakpoints were located within the segments covered by these BACs. The partial karyotype illustrates the t(7;12)(p22;q13) as seen in case 1. **b:** Physical map of 7p22, including RP11-1275H24 and RP11-93G19, flanking BAC probes and the genes *ACTB* and *FLJ11467*. The exons (**filled boxe**s) and the 5′→ 3′ orientation of the genes are indicated. BAC probe RP11-1275H24 is, based on our FISH mapping and PCR showing that the *ACTB* is present, substantially larger than the ~85 kb reported at the NCBI Nucleotide Browser (http//:www.ncbi.nlm.nih.gov). **c:** Physical map of 12q13, including RP11-181L23 and RP11-772E1, flanking BACs, and the genes *DDIT3* and *GLI1*.

The list of identified fusion genes in soft tissue neoplasms, mostly sarcomas, is steadily increasing and it has become clear that most of them involve at least one transcription factor gene.[2,3] At the molecular genetic level, the fusion of genes causes either overexpression of normally silent genes when placed under the influence of a strong promoter, or else expression of abnormal, chimeric, gene products.[2] The *ACTB-GLI* fusion gene described herein fits well with this pattern. The *ACTB* gene, encoding an important cytoskeletal component, is under the control of a conserved, strong, and complex promoter that assures a high level of expression in nonmuscle cells.[10,11] In contrast to the ubiquitous expression of *ACTB*, *GLI* expression seems to be restricted to a few tissue types, including the fallopian tube, testis, and myometrium. *GLI* is the archetype for the human *Krüppel* gene family, characterized by five DNA-binding zinc finger domains linked by highly conserved histidine-cysteine motifs.[12,13]

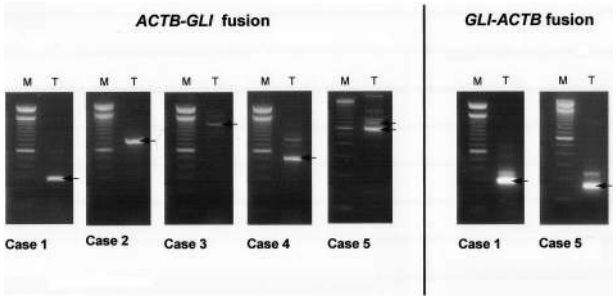

Figure 5. RT-PCR detecting *ACTB-GLI* fusion transcripts in cases 1 to 5 (case 1: ACT61F-GLI868R, 270 bp; case 2: ACT18F-GLI1246R, 754 bp; case 3: ACT61F-GLI1477R, 1172 bp; case 4: ACT61F-GLI938R, 484 bp; case 5: ACT106F-GLI868R, 610 and 712 bp), and *GLI-ACTB* fusion transcripts in cases 1and 5 (case 1: GLI520F-GLI520R, 289 bp; case 5: GLI412F-ACT520R, 162 bp). M, 100-bp ladder; T, tumor.

Activation of *GLI* genes, also including *GLI2* and *GLI3*, constitute the last known step in the *sonic hedgehog* (SHH) signaling pathway, and they thus function as direct effectors of the mediated signal. The *SHH* gene is expressed during embryogenesis and directs tissue-specific cell proliferation. Binding of SHH to the transmembrane receptor PTCH (patched) releases the repression of SMOH (smoothened) exerted by PTCH, which results in transduction of the signal.[14] The resulting activation of GLI induces an up- and down-regulation of multiple target genes involved in, eg, cell-cycle regulation, cell ad-

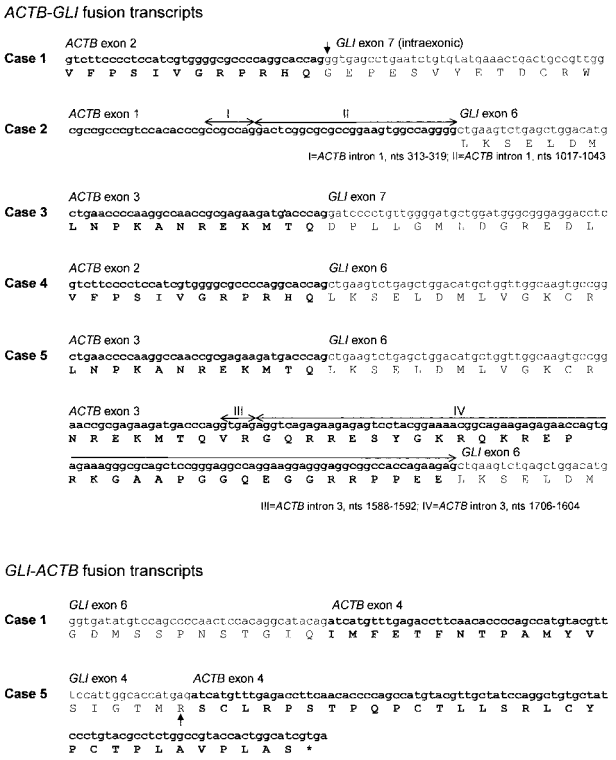

Figure 6. Partial nucleotide sequences spanning the breakpoints in the *ACTB-GLI* and *GLI-ACTB* fusion transcripts. *ACTB* sequences are highlighted in **bold characters**, and amino acids are written in **capital letters**. In case 1, the inserted guanine that maintains the open reading frame in the *ACTB-GLI* fusion is indicated (**arrow**). In case 5, the out-of-frame *GLI-ACTB* fusion leads to an S→R substitution (**arrow**) in the *GLI* sequence and ultimately to the introduction of a premature stop codon (**asterisk**). See text for details.

hesion, apoptosis, signal transduction, and cell proliferation.[15] Lack of SHH signaling during embryogenesis is associated with human developmental birth defects; mutations in *SHH* cause holoprosencephaly,[16] and *PTCH* mutations are found in patients with the Gorlin syndrome.[17] Mutations presumably leading to the inhibition of the PTCH repressor function of SMOH, or else direct activation of SMOH have been described in medulloblastoma[18,19] and basal cell carcinoma,[20,21] and overexpression of SHH has recently been described as a pathogenetic mechanism in carcinomas of the lung and upper digestive tract.[22–24] Furthermore, increased GLI activity because of amplification of the *GLI* gene has been detected in glioblastoma,[25] B-cell lymphoma,[26] and various bone and soft tissue sarcomas.[27] However, deregulation of *GLI* through fusion with another gene has not previously been described.

The complex *ACTB* promoter contains three regulatory domains, all with conserved CArG ($CC(A/T)_6GG$) *cis*-elements recognized by serum response factors. Two of them are situated upstream of the mRNA cap site, the third is found within intron 1.[11] Thus, the *ACTB-GLI* fusion transcripts detected in cases 1 and 3 to 5 should include the entire promoter region because breakpoints were located after exon 2 or 3 (Figure 1b). In case 2, however, the breakpoint was found after exon 1, and interpretation of the significance of this fusion is further complicated by the retention of *ACTB* intron 1 sequences (Figure 6). Possibly, this was because of alternative splicing mechanisms—the 697-bp fragment that was missing (nucleotides 320 to 1016, M10277) had GT-AG sequences at its boundaries. Alternatively, the *ACTB* intron 1 sequences could represent remnants of more complex changes at the genomic level, that may have led to deletion of the 13-bp consensus sequence in intron 1 (corresponding to nucleotides 933 to 947, M10277) (Figure 6).[11]

The part of *GLI* included in the *ACTB-GLI* fusion transcripts started with exon 6 (cases 2, 4, and 5), exon 7 (case 3), or from within exon 7 (case 1) (Figure 1b). Thus, the fused *GLI* sequences most likely included exons 7 to 10, which encode the five zinc finger domains,[28] four of which are DNA binding.[29] Furthermore, they should have retained sequences within exon 12 corresponding to amino acids 1020 to 1091, required for *GLI*-mediated transcriptional activation.[28,30] This transcription activation domain contains a conserved motif recognized by the human TATA box-binding protein-associated factor TAFII31, which is part of the TFIID transcription factor complex and is thought to mediate expression of *GLI* target genes.[30] Although we cannot exclude the possibility that loss of the amino terminal part of the GLI protein is of significance, eg, by affecting its subcellular localization, it is tempting to suggest that the important outcome of the detected *ACTB-GLI* fusions is that the strong *ACTB* promoter causes overexpression of *GLI* sequences important for transcriptional activation of downstream target genes. The only other sarcoma type in which a similar oncogenic mechanism has been described is dermatofibrosarcoma protuberans, where the proto-oncogene *PDGFB* is activated when put under the influence of the collagen-encoding *COL1A1* gene.[31,32]

Reciprocal *GLI-ACTB* chimeras, fusing *GLI* exon 6 to *ACTB* exon 4 in case 1, and *GLI* exon 4 to *ACTB* exon 4 in case 5, were also identified (Figure 1b), but for several reasons these are probably of little or no pathogenetic significance. First, the need for nested PCR for the detection of the reciprocal transcript supports the view of weak promoter function of *GLI* or else rapid posttranscriptional degradation. Second, in case 5, the *GLI-ACTB* fusion introduced a frame-shift in the *ACTB* sequence, and a premature stop codon (Figure 6). Third, in case 3, only the der(7)t(7;12), ie, the derivative chromosome harboring the *ACTB-GLI* fusion, but not the corresponding der(12), that should have contained the reciprocal *GLI-ACTB* fusion, could be detected.

In summary, these data support the existence of a newly identified, seemingly discrete group of soft tissue tumors that likely belong in the myopericytic category. At this time we propose the diagnostic term "pericytoma with t(7;12)" for these lesions in hopes of facilitating their definition and further recognition, but also recognizing that the most appropriate nomenclature may evolve with time after analysis of larger case numbers and better characterization of these lesions' biological potential. As a mechanistic pathway shared with many other mesenchymal neoplasms, these tumors have an, as yet, tumor-specific reciprocal translocation that results in *GLI* activation through a previously undescribed fusion with *ACTB*. These findings bring additional insight regarding

the role of *GLI* and the *SHH* signaling pathway in human neoplasia.

References

1. Fletcher CDM, Rydholm A, Singer S, Sundaram M, Coindre JM: Soft tissue tumours: epidemiology, clinical features, histopathological typing and grading. World Health Organization Classification of Tumours. Pathology and Genetics of Tumours of Soft Tissue and Bone. Edited by CDM Fletcher, KK Unni, F Mertens. Lyon, IARC Press, 2002, pp 12–18
2. Åman P: Fusion genes in solid tumors. Semin Cancer Biol 1999, 9:303–318
3. Ladanyi M, Bridge JA: Contribution of molecular genetic data to the classification of sarcomas. Hum Pathol 2000, 31:532–538
4. Perez-Atayde AR, Kozakewich HWP, McGill T, Fletcher JA: Hemangiopericytoma of the tongue in a 12-year-old child: ultrastructural and cytogenetic observations. Hum Pathol 1994, 25:425–429
5. Mandahl N: Methods in solid tumor cytogenetics. Human Cytogenetics: Malignancy and Acquired Abnormalities, ed 3. Edited by DE Rooney. New York, Oxford University Press, 2001, pp 165–203
6. ISCN: An International System for Human Cytogenetic Nomenclature. Edited by F Mitelman. Basel, Karger, 1995
7. Dahlén A, Debiec-Rychter M, Pedeutour F, Domanski HA, Höglund M, Bauer HCF, Rydholm A, Sciot R, Mandahl N, Mertens F: Clustering of deletions on chromosome 13 in benign and low-malignant lipomatous tumors. Int J Cancer 2003, 103:616–623
8. McMenamin ME: Myopericytoma. World Health Organization Classification of Tumours. Pathology and Genetics of Tumours of Soft Tissue and Bone. Edited by CDM Fletcher, KK Unni, F Mertens. Lyon, IARC Press, 2002, pp 138–139
9. Guillou L, Fletcher JA, Fletcher CDM, Mandahl N: Extrapleural solitary fibrous tumour and haemangiopericytoma. World health Organization Classification of Tumours. Pathology and Genetics of Tumours of Soft Tissue and Bone. Edited by CDM Fletcher, KK Unni, F Mertens. Lyon, IARC Press, 2002, pp 86–90
10. Ng S-Y, Gunning P, Eddy R, Ponte P, Leavitt J, Shows T, Kedes L: Evolution of the functional human β-actin gene and its multi-pseudogene family: conservation of noncoding regions and chromosomal dispersion of pseudogenes. Mol Cell Biol 1985, 5:2720–2732
11. Ng S-Y, Gunning P, Liu S-H, Leavitt J, Kedes L: Regulation of the human β-actin promoter by upstream and intron domains. Nucleic Acids Res 1989, 17:601–615
12. Kinzler KW, Ruppert JM, Bigner SH, Vogelstein B: The GLI gene is a member of the Kruppel family of zink finger proteins. Nature 1988, 332:371–374
13. Kinzler KW, Vogelstein B: The GLI gene encodes a nuclear protein which binds specific sequences in the human genome. Mol Cell Biol 1990, 10:634–642
14. Villavicencio EH, Walterhouse DO, Iannaccone PM: The sonic hedgehog-patched-gli pathway in human development and disease. Am J Hum Genet 2000, 67:1047–1054
15. Yoon JW, Kita Y, Frank DJ, Majewski RR, Konicek BA, Nobrega MA, Jacob H, Walterhouse D, Iannaccone P: Gene expression profiling leads to identification of GLI1 binding elements in target genes and a role for multiple downstream pathways in GLI1-induced cell transformation. J Biol Chem 2002, 7:5548–5555
16. Roessler E, Belloni E, Gaudenz K, Jay P, Berta P, Scherer SW, Tsui LC, Muenke M: Mutations in the human Sonic Hedgehog gene cause holoprosencephaly. Nat Genet 1996, 14:357–360
17. Hahn H, Wicking C, Zaphiropoulos PG, Gailani MR, Shanley S, Chidambaram A, Vorechovsky I, Holmberg E, Unden AB, Gillies S, Negus K, Smyth I, Pressman C, Leffell DJ, Gerrard B, Goldstein AM, Dean M, Toftgard R, Chenevix-Trench G, Wainwright B, Bale AE: Mutations in the human homolog of drosophila patched in the nevoid basal cell carcinoma syndrome. Cell 1996, 85:841–851
18. Raffel C, Jenkins RB, Frederick L, Hebrink D, Alderete B, Fults DW, James CD: Sporadic medulloblastomas contain PTCH mutations. Cancer Res 1997, 57:842–845
19. Reifenberger J, Wolter M, Weber RG, Magahed M, Ruzicka T, Lichter P, Reifenberger G: Missense mutations in SMOH in sporadic basal cell carcinomas of the skin and primitive neuroectodermal tumors of the central nervous system. Cancer Res 1998, 58:1798–1803
20. Unden AB, Holmberg E, Lundh-Rozell B, Ståhle-Bäckdahl M, Zaphiropoulos PG, Toftgård R, Vořechovsky I: Mutations in the human homologue of drosophila patched (PTCH) in basal cell carcinomas and the Gorlin syndrome: different in vivo mechanisms of PTCH inactivation. Cancer Res 1996, 56:4562–4565
21. Xie J, Murone M, Luoh S-M, Ryan A, Gu Q, Zhang C, Bonifas JM, Lam C-W, Hynes M, Goddard A, Rosenthal A, Epstein Jr EH, de Sauvage FJ: Activating Smoothened mutations in sporadic basal-cell carcinoma. Nature 1998, 391:90–92
22. Berman DM, Karhadkar SS, Maitra A, Montes de Oca R, Gerstenblith MR, Briggs K, Parker AR, Shimada Y, Eshleman JR, Watkins DN, Beachy PA: Widespread requirement for Hedgehog ligand stimulation in growth of digestive tract tumours. Nature 2003, 425:846–851
23. Thayer SP, Pasca di Magliano M, Heiser PW, Nielsen CM, Roberts DJ, Lauwers GY, Ping Qi Y, Gysin S, Fernández-del Castillo C, Yajnik V, Antoniu B, McMahon M, Warshaw AL, Hebrok M: Hedgehog is an early and late mediator of pancreatic cancer tumorigenesis. Nature 2003, 425:851–856
24. Watkins DN, Berman DM, Burkholder SG, Wang B, Beachy PA, Baylin SB: Hedgehog signalling within airway epithelial progenitors and in small-cell lung cancer. Nature 2003, 422:313–317
25. Kinzler KW, Bigner SH, Bigner DD, Trent JM, Law ML, O'Brien SJ, Wong AJ, Vogelstein B: Identification of an amplified, highly expressed gene in a human glioma. Science 1987, 236:70–73
26. Werner CA, Döhner H, Joos S, Trűmper LH, Baudis M, Barth TFE, Ott G, Möller P, Lichter P, Bentz M: High-level DNA amplifications are common genetic aberrations in B-cell neoplasms. Am J Pathol 1997, 151:335–342
27. Stein U, Eder C, Karsten U, Haensch W, Walther W, Schlag PM: GLI gene expression in bone and soft tissue sarcomas of adult patients correlates with tumor grade. Cancer Res 1999, 59:1890–1895
28. Liu CZ, Yang JT, Yoon JW, Villavicencio E, Pfendler K, Walterhouse D, Iannaccone P: Characterization of the promoter region and genomic organization of GLI, a member of the Sonic hedgehog-Patched signaling pathway. Gene 1998, 209:1–11
29. Pavletich NP, Pabo CO: Crystal structure of a five-finger GLI-DNA complex: new perspectives on zinc fingers. Science 1993, 261:1701–1707
30. Yoon JW, Liu CZ, Yang JT, Swart R, Iannaccone P, Walterhouse D: GLI activates transcription through a herpes simplex viral protein 16-like activation domain. J Biol Chem 1998, 6:3496–3501
31. Simon M-P, Pedeutour F, Sirvent N, Grosgeorge J, Minoletti F, Coindre J-M, Terrier-Lacombe M-J, Mandahl N, Craver RD, Blin N, Sozzi G, Turc-Carel C, O'Brien K, Kedra D, Fransson I, Guilbaud C, Dumanski JP: Deregulation of the platelet-derived growth factor B-chain gene via fusion with collagen gene COL1A1 in dermatofibrosarcoma protuberans and giant cell fibroblastoma. Nat Genet 1997, 15:95–98
32. O'Brien KP, Seroussi E, Dal Cin P, Sciot R, Mandahl N, Fletcher JA, Turc-Carel C, Dumanski JP: Various regions within the alpha-helical domain of the COL1A1 gene are fused to the second exon of the PDGFB gene in dermatofibrosarcomas and giant-cell fibroblastomas. Genes Chromosomes Cancer 1998, 23:187–193